AIAA 2000-0285

Acoustic Source for Compressible Flow Receptivity Experiments

J. D. Schmisseur, J. Poggie, and R. L. Kimmel
Air Force Research Laboratory
Wright-Patterson AFB, OH 45433-7521

38th Aerospace Sciences Meeting & Exhibit
10-13 January 2000/Reno, NV

Acoustic Source for Compressible Flow Receptivity Experiments

J. D. Schmisseur*
J. Poggie*
R. L. Kimmel†
US Air Force Research Laboratory
Wright-Patterson AFB, OH 45433-7521

An experimental program has been undertaken to examine the receptivity of compressible boundary layer flows to acoustic disturbances. Preliminary work has focused on identifying a suitable acoustic source and characterizing the disturbance field induced in supersonic flow over a flat plate. Pressure measurements were made, and compared to the acoustic theory for a harmonic point source in inviscid, supersonic flow. The theory predicts that the superposition of the fast and slow components of the disturbance field leads to a complex interference pattern, contained within the Mach cone emanating from the acoustic source. The amplitude and phase of the experimental acoustic field were extracted from the data using two methods: conditional averaging in the time domain and cross-spectral analysis in the frequency domain. Where good signal-to-noise ratio was obtained, the methods were found to agree, and the shape of the theoretical amplitude and phase distributions was resolved experimentally.

Nomenclature

Roman Symbols

a	= sound speed
A	= amplitude
D	= nondimensional parameter
f	= frequency
G	= one-sided spectrum
$\Im$	= imaginary part of complex number
M	= Mach number
N	= natural logarithm of disturbance amplitude ratio
p	= pressure
q	= mass flux
R	= distance
$\Re$	= real part of complex number
Re_x	= Reynolds number: $U_\infty x/\nu_\infty$
t	= time
T	= temperature or signal record duration
u,v,w	= streamwise, wall-normal, and spanwise velocity components
V	= freestream speed
x,y,z	= streamwise, wall-normal, and spanwise coordinates

Greek Symbols

γ^2	= coherence derived from cross-spectrum
δ	= boundary layer thickness
θ	= angle
λ	= wavelength
ν	= kinematic viscosity
τ	= time delay between detection of event at each sensor
ϕ	= phase
ω	= angular frequency

Subscripts

e	= boundary layer edge conditions
w	= wall conditions
S	= acoustic source
0	= stagnation conditions
∞	= freestream conditions

Superscripts

$*$	= complex conjugate
$\hat{}$	= Fourier transform

*Research Aerospace Engineer, Air Vehicles Directorate, AFRL/VAAC, BLDG 146 RM 225, 2210 EIGHTH ST, Senior Member AIAA.

†High Speed Team Leader, Air Vehicles Directorate, AFRL/VAAA, 2130 EIGHTH ST STE 1, Associate Fellow AIAA.

Introduction

ALL methods currently in common use for predicting transition are correlations. Even the most sophisticated of these, the e^N method, based on linear stability theory, relies on an empirical correlation between the location of transition and the N-factor. Unless the flow to be predicted is identical to the flow on which the correlation is based, such methods have an inherently high degree of uncertainty. For example, the correlating N-factor typically lies between about

eight and thirteen for external flows in aerospace applications, with nine often taken as a nominal value.

The recent development of tools to predict disturbance growth in the nonlinear regime opens the possibility of a rational, amplitude-based method of transition prediction. For example, in methods based on the Parabolized Stability Equations (PSE), the disturbance amplitude is computed from inception, nonlinear interactions are tracked, and the point of initial mean flow distortion is identified as the onset of transition. Similarly, direct numerical simulation (DNS) has been used to study the full nonlinear response of a flow to the disturbance environment. Such methods hold promise for predicting transition from first principles, without resort to empiricism.

The first step in this approach is determining the disturbance amplitude at the initial condition of the computation. For direct numerical simulations, these disturbances would ideally be related to a freestream turbulence spectrum measured in the atmosphere. In practical DNS computations, and in approximate methods like the PSE, knowledge of the initial disturbance in the boundary layer may be needed.

In general, the initial amplitude of a boundary layer disturbance will not be equal to the freestream disturbance amplitude. For example, the amplitude of an acoustic wave reflecting from a surface in the presence of a boundary layer depends (among other factors) on λ/δ, the ratio of the acoustic wavelength to the boundary layer thickness.[1] 'Receptivity' is a term used to describe the sensitivity of the boundary layer to background fluid dynamic and thermodynamic disturbances.[2]

One approach to determining the initial disturbance amplitude in the boundary layer is to compute the forced response of the stable portion of the flow up to the lower neutral bound, then to take that disturbance amplitude as the starting point for a conventional computation of the free response downstream.[3] In general, however, forced disturbances have neither dispersion relations matching those of the free boundary layer instabilities, nor amplitude distributions matching the linear stability eigenfunctions. Some matching process or energy redistribution between the imposed background disturbances and the boundary layer instabilities must take place.

These issues have been addressed using asymptotic analysis, which shows that strong excitation occurs when disturbances generated by nonlinear interaction of external waves and wall-induced disturbances are in resonance with the normal mode waves.[4] In particular, the receptivity of the boundary layer is different for fast and slow acoustic waves.

The goal of our research program is to experimentally characterize the acoustic receptivity of a hypersonic boundary layer, and to provide a benchmark experiment for code validation. Relatively little experimental work has been done heretofore in this area.[5–7] The first step in this task is to develop a generator capable of creating suitable acoustic waves in a supersonic flow; in recent work we have identified piezo-ceramic ultrasonic transducers as a candidate.[8] Since the receptivity of a hypersonic boundary layer to acoustic waves depends on the frequency, wave angle, and phase velocity of the incoming wave, one requirement of the acoustic generator is to produce a suitable frequency / wavenumber spectrum. This paper describes detailed measurements of the acoustic field downstream of an ultrasonic point source embedded in a flat plate in supersonic flow. These initial experiments were carried out in a conventional wind tunnel, with turbulent sidewall boundary layers, so no receptivity measurements were made. In future work, we hope to be able to carry out further experiments in a quiet, laminar-flow facility.

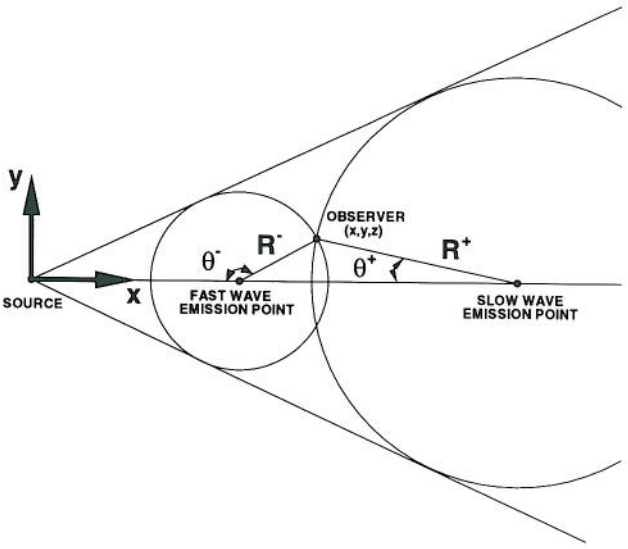

Fig. 1 Acoustic point source in supersonic cross-flow.

Theory

For a relatively thin boundary layer on a flat plate, the acoustic field induced by the ultrasonic transducer should be similar to that induced by a point source in a uniform supersonic flow. Morse and Ingard[9] present the solution for the related case of a point source traveling at supersonic speed. In that problem, the pressure at a given time and point within the Mach cone downstream of the source is given by the superposition of the fast and slow acoustic wavefronts emitted by the source at two different times (and thus positions) in the past. A coordinate transformation can be used to adapt this solution to the case of a fixed point source in a supersonic cross-stream.

For the fixed source, the pressure field is given by:

$$p = -\frac{q'(t^+)}{4\pi R^+ (D^+)^2} + \frac{q'(t^-)}{4\pi R^- (D^-)^2}$$

$$-\frac{q(t^+)VN^+}{4\pi(R^+)^2(D^+)^3}+\frac{q(t^-)VN^-}{4\pi(R^-)^2(D^-)^3} \quad (1)$$

where $M = V/a$, $t^\pm = t - R^\pm/a$, $N^\pm = M - \cos\theta^\pm$, and $D^\pm = M\cos\theta^\pm - 1$.

The quantities

$$R^\pm = \frac{Mx \pm \sqrt{x^2-(M^2-1)(y^2+z^2)}}{(M^2-1)} \quad (2)$$

represent the distance from the current location of the observer, (x, y, z), to the current location of the fluid particle that coincided with the source when the wavefront was emitted. The corresponding angles from the line of symmetry are:

$$\theta^+ = \arcsin(\sqrt{y^2+z^2}/R^+) \quad (3)$$

$$\theta^- = \pi - \arcsin(\sqrt{y^2+z^2}/R^-) \quad (4)$$

These quantities are shown geometrically in Fig. 1.

The function $q(t)$ represents the total rate of mass flux out of the source. The terms in Eq. (1) containing $q'(t)$ are formally identical to the equation for the acoustic field from a stationary point source (which decays with distance away from the source as $1/R$), with the additional scaling term $(D^\pm)^{-2}$. The quantities containing q are additional terms arising from the relative motion of the source and observer.

All disturbances are contained within the Mach cone emanating from the source (see Fig. 1). At any point within the Mach cone, the amplitude of the acoustic field is a superposition of two waves, one from the leading 'fast' $(u+a)$ portion of the acoustic wave, and the other from the 'slow' $(u-a)$ trailing portion of the wave. This leads to complex interference patterns, which will be illustrated below.

For a harmonic source, $q(t) = q_0 e^{-i\omega t}$ and $q'(t) = -i\omega q_0 e^{-i\omega t}$. The corresponding pressure field is:

$$p = q_0 e^{-i\omega t}\left[-\frac{i\omega e^{ik^+}}{4\pi R^+(D^+)^2}+\frac{i\omega e^{ik^-}}{4\pi R^-(D^-)^2} -\frac{e^{ik^+}VN^+}{4\pi(R^+)^2(D^+)^3}+\frac{e^{ik^-}VN^-}{4\pi(R^-)^2(D^-)^3}\right] \quad (5)$$

where $k^\pm = \omega R^\pm/a$. This equation can be re-written in the form:

$$p(x,y,z,t) = A(x,y,z)\exp[-i(\omega t - \phi(x,y,z))] \quad (6)$$

In this form, the acoustic field can be considered to be a time-periodic disturbance at the same frequency as the source, with an amplitude and phase modulation in space.

Example plots were generated for a case corresponding to the experimental conditions: $M = 2.8$, $f_S = 28$ kHz, and $T_0 = 280$ K. Figure 2 shows the amplitude distribution, $A(x, y, 0)$, created by the point source. (Since the amplitude becomes infinite at the Mach wave, the contours are truncated for clarity at a value of 5.) Looking along a line perpendicular to the Mach cone, we first see a jump across the shock from the undisturbed freestream to a very large value (infinite in the context of Eq. 5). The amplitude decays rapidly with distance from the shock, passing through a series of maxima and minima due to the interference of the fast and slow components of the pressure field.

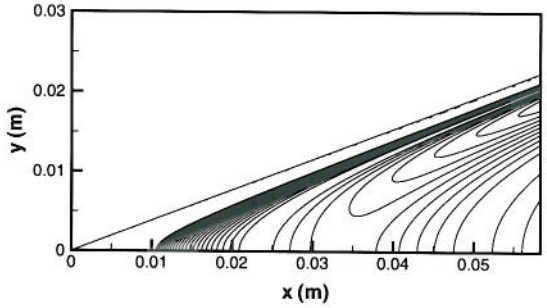

Fig. 2 Contours of amplitude downstream of a point source in supersonic flow. Contour interval 0.2, amplitude referenced to value at $x \approx 0.02$ m.

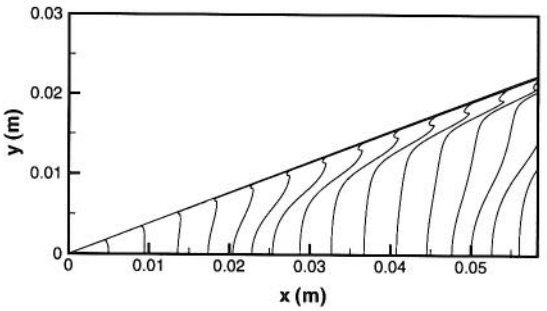

Fig. 3 Contours of unwrapped phase downstream of a point source in supersonic flow. Contour interval $\pi/2$.

The corresponding phase distribution was computed by applying the Fortran function **ATAN2** to the real and imaginary parts of the term in brackets in Eq. (5), giving an angle in the range $-\pi \le \phi \le \pi$. Since **ATAN2** is arbitrary to multiples of 2π, discontinuities in the

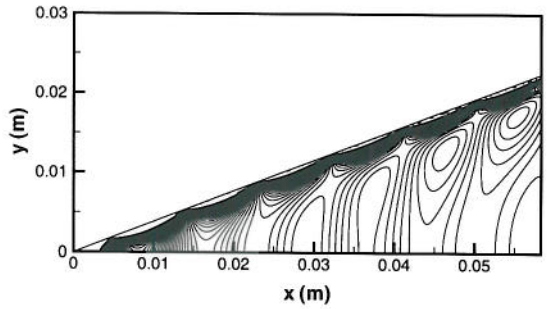

Fig. 4 Contours of instantaneous pressure perturbation downstream of a point source in supersonic flow. Contour interval 1, amplitude referenced to value at $x \approx 0.02$ m.

phase distribution were eliminated by searching along rays from the origin and adding a multiple of 2π every time a jump occurred. This kind of unwrapping makes phase plots considerably less cluttered, and is physically meaningful because the unwrapped phase is directly related to the time delay for signal propagation. The resulting phase distribution, $\phi(x, y, 0)$, is shown in Fig. 3. There are sharp changes in the phase distribution corresponding to the extrema in the amplitude distribution, again corresponding to the interference patterns of the fast and slow waves.

The instantaneous pressure perturbation, $p(x, y, 0, t_1)$, was evaluated for $t_1 = 5$ s, and is shown in Fig. 4. The instantaneous perturbation has a different character than the amplitude and phase distributions. The time modulation introduces a number of maxima and minima, corresponding to constructive and destructive interference of the instantaneous fast and slow waves. In a time-history of the pressure perturbation field, these structures would appear to propagate away from the source.

Experimental Methods

The measurements were made in the test section of the Air Force Institute of Technology (AFIT) Mach 3 wind tunnel. The AFIT tunnel is a blowdown facility with run times on the order of 30 s, limited by the volume of the vacuum vessels into which the flow is exhausted. The square 63.5 mm by 63.5 mm test section is 330 mm long, and begins 270 mm downstream of the nozzle throat. Instrument access is provided through slots in the floor and ceiling of the test section, while optical access is provided through round glass windows spanning the height of the test section in the test section walls. Photographs of the facility

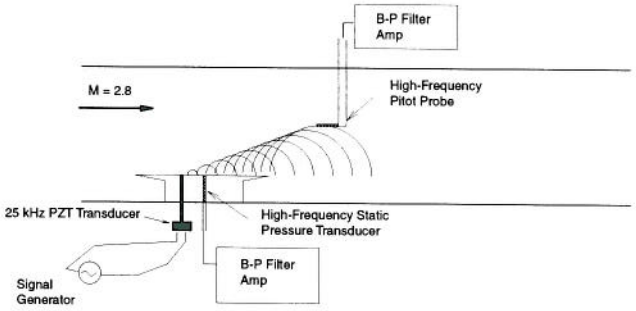

Fig. 5 Schematic of experiment.

have been presented elsewhere.[8,10]

For the present experiment the tunnel stagnation pressure and temperature were 250±6 kPa (36±1 psia) and 280 K (nominal), respectively. Using the measured test section Mach number of 2.8 reported by Tilmann,[10] the unit Reynolds number corresponding to the above stagnation conditions is 20×10^6 m^{-1} and the freestream velocity is 600 m/s. Tilmann[10] reports a boundary-layer thickness of 5.3 mm on the tunnel ceiling 55.8 mm downstream of the start of the test section at a unit Reynolds number of 17×10^6 m^{-1} to 18×10^6 m^{-1}.

The experimental model was a flat plate 83.5 mm long by 62 mm wide, positioned 25 mm downstream from the start of the test section. The plate was mounted 21 mm above the floor of the tunnel using a pylon in the shape of a diamond airfoil (see Fig. 5). The acoustic disturbances were introduced into the flow through a 3 mm diameter hole, located 25.2 mm downstream from the leading edge of the plate. The sound source was a 16 mm diameter piezo-ceramic transducer (manufactured by APC corporation) connected to the plate by a wave guide in the model support pylon.

The ultrasonic transducer is designed to emit a monochromatic acoustic signal, nominally at 25 kHz, when driven by an excitation voltage of the same frequency. Bench-top tests of the transducer used in the present experiments indicated that, for a sinusoidal input signal, the maximum output occurs at a frequency of 28 kHz. Bench tests also verified the manufacturer's specification of a sound pressure level, under atmospheric conditions, of 112 dB at a distance of 300 mm from the source. Assuming a reference pressure of 20 μPa, this sound intensity corresponds approximately to a 8 Pa root-mean-square pressure fluctuation. For the present work, the ultrasonic transducers were driven with a 28 kHz sine wave produced by a function generator.

Instrumentation

The effect of the acoustic excitation on the flowfield was measured using high-frequency pressure transducers. Static pressure fluctuations were measured with an Entran 541 2 psid (14 kPa) pressure transducer,

referenced to a pressure of 0.44 psia (3.0 kPa) maintained in a small vacuum chamber near the facility. The transducer was flush-mounted in the flat plate surface 19.7 mm downstream of the acoustic source. Pitot pressure fluctuations were measured with a Kulite model XCW-093 5 psid (34 kPa) pressure transducer referenced to atmospheric pressure and mounted in a Pitot probe extending through the test section ceiling.

The signals from the pressure transducers were amplified with a gain of 100 using a custom signal conditioning circuit. The signals were then band-pass filtered with Stanford Research Systems model 650 dual channel filters. The use of a 27-29 kHz pass band was found to effectively suppress both broadband noise and 'ringing' at the natural frequencies of the transducer.

The analog signals were digitized with 8 bit resolution at a sampling rates of 1 MHz using a LeCroy model 9384 CTM oscilloscope. Three channels of data (excitation and two pressure signals) were collected simultaneously in segmented records. A typical run consisted of 468 segments of 1002 points with the start of a new segment synchronized to a trigger event.

Signal Processing

The main signal processing issue in boundary layer receptivity work is the difficulty in distinguishing the response of the flow to the input forcing from the background disturbance level in the measuring system and in the flow (due to acoustic noise generated, for example, by the turbulent side-wall boundary layers and mechanical vibration). Various kinds of averaging can be used to eliminate random noise from the desired coherent response signal.

Lock-in averaging, or phase-averaging, can be used for periodic inputs. The signal in the time-domain is averaged continuously over the period of the input. This method rejects all frequencies other than the input frequency and its harmonics, as well as that portion of the output signal that is not phase-locked to the input.

Since each data segment captured by the oscilloscope was triggered at the same phase of the excitation sine wave, the data set could be phase-averaged in a straight-forward manner. (Here we average over several periods of the input, see Fig. 7.) All 468 data segments collected during the run were averaged, and the resulting mean signal was Fourier transformed. The amplitude and phase of the transformed signal were extracted at the excitation frequency, and relative amplitude and phase between the probe signal and the plate signal were determined by division and subtraction, respectively.

The cross-spectrum between the input and the output can also distinguish the boundary layer response from the background noise. Assuming the boundary layer disturbances have sufficiently small amplitude to be in the linear regime, the coherence indicates the fraction, at a given frequency, of the output's mean square value that is contributed by the input. The phase indicates the average phase difference at each frequency between the two signals.

Assuming that the flow in the receptivity experiments corresponds approximately to a linear system with no input noise and uncorrelated output noise, techniques from linear systems theory can be used to process the data.[11] The linear frequency response function for this case is defined as the cross-spectrum divided by the auto-spectrum of the input signal:

$$H(f) = G_{xy}(f)/G_{xx}(f) \tag{7}$$

where f is restricted to the band where G_{xx} is non-zero. If the input signal is a sine wave, as in the present experiments, H can be found for a single frequency. For a broad-band input, an estimate of H can be obtained from a single experiment.

The magnitude of H can be interpreted as a gain factor. Since G_{xx} is real, the phase of the frequency response function is the same as that of the cross-spectrum: the phase difference between the input and output at each frequency.

The frequency response function was computed from the cross-spectrum between the signal from the transducer in the plate and that from the transducer in the Pitot probe. In the linear regime, the background noise is uncorrelated with the flow response to the excitation, so it is permissible to subtract a cross-spectrum of the noise obtained with the excitation off from the cross-spectrum obtained with the excitation on to obtain an improved estimate of the response to the excitation.

Results

Basic Results

Examples of the auto-spectrum of the signal from the transducer mounted in the plate are shown in Fig. 6. The spectrum for the case with the excitation off reflects the effect of the band-pass filter on the spectrum of the broad-band noise present in the background flow. In the absence of filtering, a relatively flat background spectrum is present. With the filters on, all data outside the range of 27-29 kHz are suppressed.

With the excitation on, a strong spike appears in the vicinity of 28 kHz. (Checks were made to ensure that this spike did not represent electronic cross-talk.) An estimate of the spectrum due to the excitation alone can be obtained by subtracting the case with excitation off from the case with excitation on. The signal-to-noise ratio is seen to be less than one; this is typical of the data set.

A significant improvement in the effective signal-to-noise ratio was obtained by conditional averaging

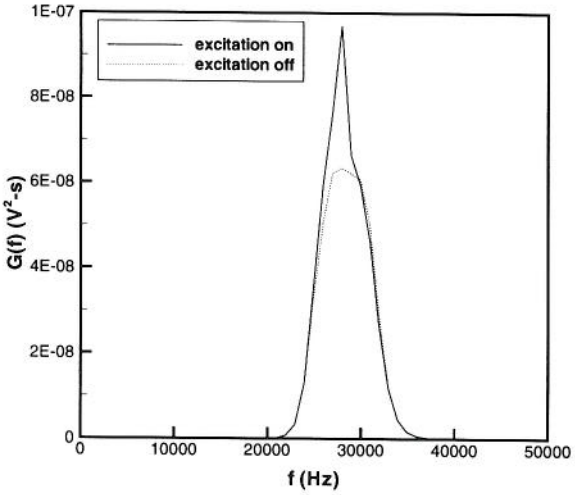

Fig. 6 Example auto-spectra for transducer mounted in plate; $x = 0.02$ m, $y = 0$ m.

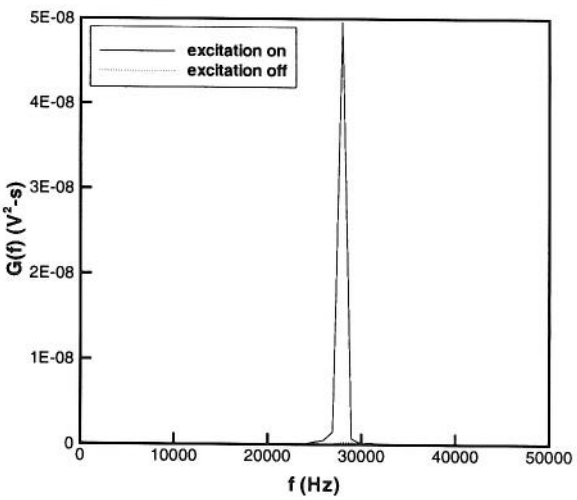

Fig. 8 Spectrum of phase-averaged signal; $x = 0.02$ m, $y = 0$ m.

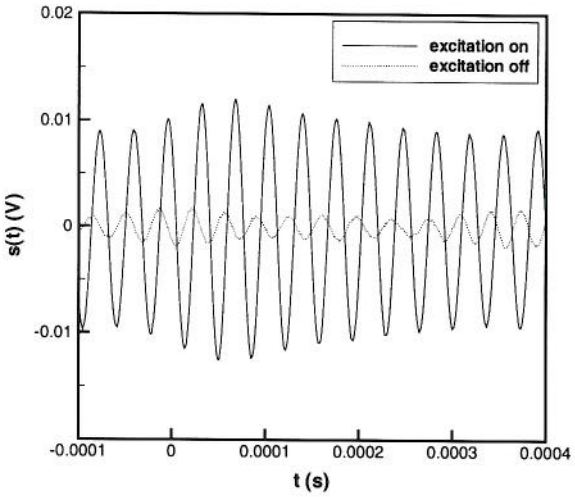

Fig. 7 Phase-averaged signal; $x = 0.02$ m, $y = 0$ m.

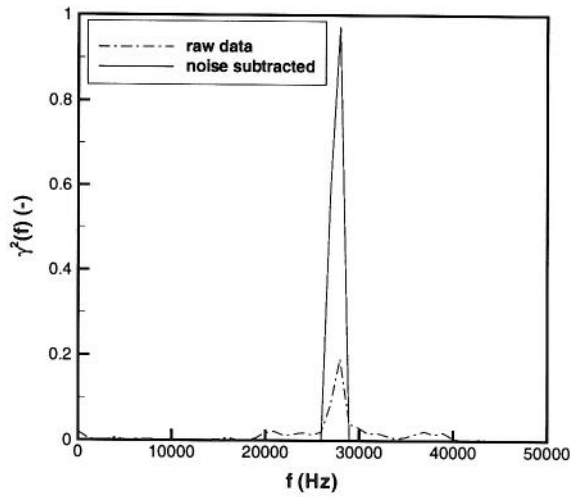

Fig. 9 Coherence of signal. Plate transducer: $x = 0.02$ m, $y = 0$ m; Probe transducer: $x = 0.02$ m, $y = 0.007$ m

methods. These included phase averaging in both the time and frequency domains.

Figure 7 shows the time-domain phase-average of the same signal. The low-frequency modulation apparent in the results is an artifact of the band-pass filtering used to reduce extraneous noise. With the filters on, signal components with a period on the order of the length of the signal ($T \approx 2$ ms or $f \approx 500$ Hz) are strongly attenuated. The amplitude of the signal with the excitation on is significantly greater than that with the excitation off, indicating an improvement in the signal-to-noise ratio with time-domain phase-averaging.

The corresponding power spectrum is shown in Fig. 8. The improvement in signal-to-noise ratio with phase averaging is quite striking in this plot. The case with the excitation on has the form of a spike near 28 kHz. In contrast, the background spectrum is almost invisible.

Similar improvements can be obtained in cross-spectral statistics by subtracting the cross-spectrum of the background noise from the cross-spectrum of the signal with excitation. An example, the coherence between the signals from the transducer in the plate and the transducer in the Pitot probe, is shown in Fig. 9. For the raw data, the peak coherence γ^2 is less than 0.2; with noise subtraction the coherence at the excitation frequency approaches 1.0.

Surveys

A series of surveys along the horizontal and vertical directions was carried out with the Pitot probe. Simul-

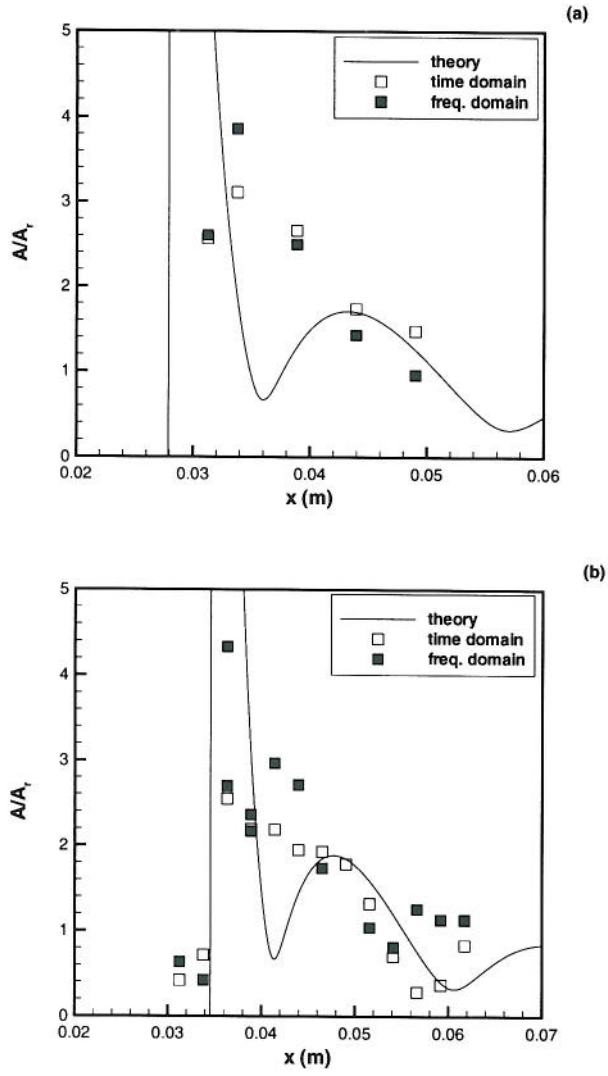

Fig. 10 Relative amplitude from streamwise survey. (a) $y = 10.7$ mm (0.42 in). (b) $y = 13.2$ mm (0.52 in).

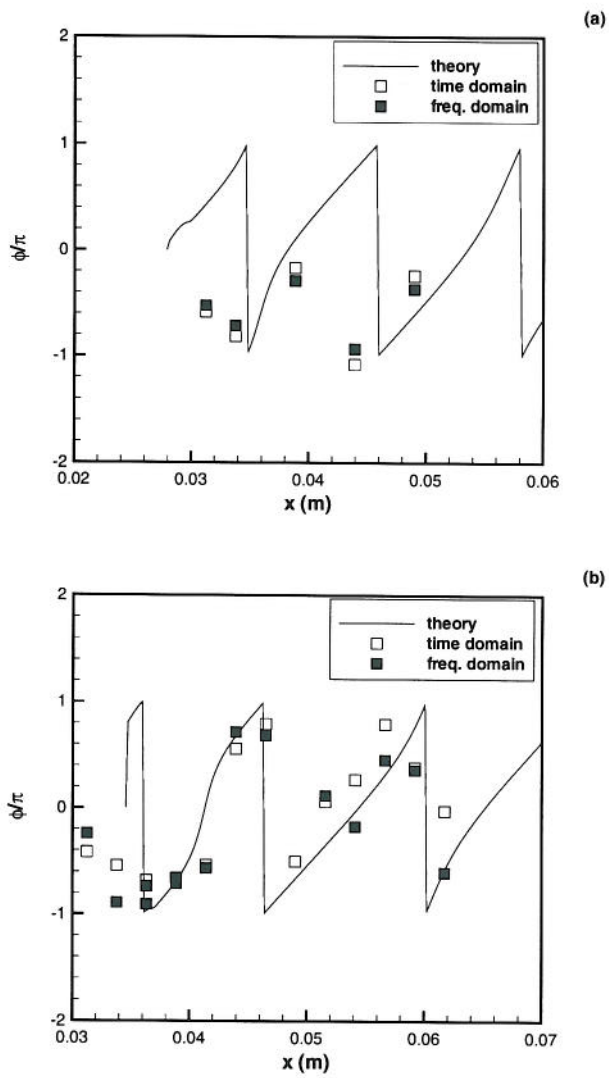

Fig. 11 Streamwise survey of relative phase. (a) $y = 10.7$ mm (0.42 in). (b) $y = 13.2$ mm (0.52 in).

taneous signals were recorded from the excitation voltage, static pressure transducer, and Pitot probe. As discussed previously, the amplitude and phase of the Pitot probe signal relative to the static pressure transducer signal were computed using both time-domain and frequency-domain averaging. As will be shown, the two methods gave results that agreed within the uncertainty of the measurements.

Streamwise surveys were carried out at heights of 10.7 mm (0.42 in) and 13.2 mm (0.52 in) above the plate. The amplitude distributions are shown in Fig. 10. The reference amplitude has been adjusted to match the data and the theory. For this reason, only the shapes of the curves, and not the absolute values, can legitimately be compared.

Similar results were obtained at both vertical stations. As discussed previously, the theory predicts an initial jump across the Mach wave (vertical line at the left of each plot) from the undisturbed freestream to a large value downstream, which decays with distance from the Mach wave through a series of maxima and minima. Considerable scatter exists in the experimental data because of a poor signal-to-noise ratio, and the first minimum downstream of the shock was not resolved experimentally. (This discrepancy could also be an effect of the finite size of the source in the experiments; the theory assumes an infinitesimal point source.) Nevertheless, there is general agreement between theory and experiment in the trend of decreasing amplitude downstream of the shock.

The corresponding results for the phase are shown in Fig. 11. The phase was not unwrapped here, so jumps of 2π are evident in the plot. Both the data from the time-domain and the frequency-domain analyses are in reasonable agreement with the theory, although there is significant scatter.

Surveys along the wall-normal direction were car-

ried out at distances of 19.8 mm (0.78 in), 60.5 mm (2.38 in), and 64.3 mm (2.53 in) downstream of the acoustic source. The distributions of relative amplitude are shown in Figure 12. Again, the reference amplitude has been adjusted to match the data and theory, so only the shapes of the curves can legitimately be compared.

The level of agreement between experiment and theory is similar to that obtained in the streamwise surveys. One important difference is that the first few relative maxima and minima behind the Mach wave are resolved in Figs. 12b and 12c. This result may be associated with improved signal-to-noise ratio at these stations.

The corresponding profiles of the phase are shown in Fig. 13. For the survey at $x = 19.8$ mm, Fig. 13a, the theory predicts an essentially uniform phase profile. The corresponding data show a high degree of scatter. Better agreement between theory and experiment is seen in the other two profiles, Figs. 13b and 13c, especially toward the middle of the profiles, where the signal was strongest relative to the noise.

Conclusions

An experimental program has been undertaken to examine the receptivity of compressible boundary layer flows to acoustic disturbances. Preliminary work has focused on identifying a suitable acoustic source and characterizing the disturbance field induced in supersonic flow over a flat plate. Some initial pressure measurements were made, and compared to the acoustic theory for a harmonic point source in inviscid, supersonic flow.

The theory predicts that the superposition of the fast and slow components of the disturbance field leads to a complex interference pattern, contained within the Mach cone emanating from the acoustic source. In particular, the amplitude induced by the source decays, through a series of local maxima and minima, from a large value at the Mach wave. Rapid changes in the phase distribution occur near the extrema in the amplitude distribution. Despite the relative complexity of the generated acoustic field, it is a well-understood, linear phenomenon, and an acoustic point source should prove to be a suitable disturbance source for compressible flow receptivity experiments.

The amplitude and phase of the experimental acoustic field were extracted from the data using two methods: conditional averaging in the time domain and cross-spectral analysis in the frequency domain. The methods were found to agree within the scatter in the results. Where good signal-to-noise ratio was obtained, the maxima and minima in the theoretical amplitude distribution were resolved experimentally, as was the shape of the phase distribution.

A number of approaches could be used in future experiments to address the issue of signal-to-noise ratio. More records could be averaged to reduce the random error in the signal analysis, and longer records would improve the frequency resolution. The pressure transducers used in the present work are designed to measure much larger fluctuations than encountered here (up to 190 dB referenced to 20 μPa), but more sensitive transducers have a more limited useful frequency range under these experimental conditions. It may be more productive to measure another variable representative of the flow disturbances, such as velocity, with a hot-wire probe.

Acknowledgments

This project was sponsored by the Air Force Office of Scientific Research, and monitored by S. Walker. S. Schneider of Purdue University designed and provided circuit boards for the dynamic pressure transducer signal amplifiers, and G. Buck of the South Dakota School of Mines and Technology contributed significantly to the initial stages of this project. We are indebted to the AFIT staff for assistance in carrying out the experiments.

References

[1]Mack, L. M., "Boundary-Layer Linear Stability Theory," *Special Course on Stability and Transition of Laminar Flow*, edited by R. Michel, No. R-709 in AGARD Reports, NATO Advisory Group for Aerospace Research and Development, Neuilly Sur Seine, France, 1984, pp. 3–1–3–81.

[2]Morkovin, M. V., "On the Many Faces of Transition," *Viscous Drag Reduction*, edited by C. S. Wells, Plenum Press, New York, 1969.

[3]Mack, L. M., "Linear Stability Theory and the Problem of Supersonic Boundary Layer Transition," *AIAA Journal*, Vol. 13, No. 3, 1975, pp. 278–289.

[4]Fedorov, A. V., "Receptivity of Hypersonic Boundary Layer to Acoustic Disturbances Scattered by Surface Roughness," Final Report MIPT/FALT-1999-015, European Office of Aerospace Research and Development, London, UK, July 1999.

[5]Kendall, J. M., "Wind Tunnel Experiments Relating to Supersonic and Hypersonic Boundary-Layer Transition," *AIAA Journal*, Vol. 13, No. 3, 1975, pp. 290–299.

[6]Semionov, N. V., Kosinov, A. D., and Maslov, A. A., "Experimental Investigation of Supersonic Boundary-Layer Receptivity," *Transitional Boundary Layers in Aeronautics*, edited by R. A. W. M. Henkes and J. L. van Ingen, Royal Netherlands Academy of Arts and Sciences, Amsterdam, 1996, pp. 413–420.

[7]Maslov, A. A., Shiplyuk, A. N., Sidorenko, A. A., and Arnal, D., "Leading Edge Receptivity of the Hypersonic Boundary Layer on a Flat Plate," ITAM Preprint 1-98, Institute of Theoretical and Applied Mechanics, Russian Academy of Sciences, Siberian Branch, Novosibirsk, Russia, 1998.

[8]Buck, G. A., Kimmel, R. L., and Schmisseur, J. D., "Characterization of Acoustic Sources for Hypersonic Receptivity Research," AIAA Paper 99-3708, June 1999.

[9]Morse, P. M. and Ingard, K. U., *Theoretical Acoustics*, Princeton University Press, Princeton, NJ, 1986.

[10]Tilmann, C. P., *Numerical and Experimental Investigation of the Flowfield Near a Wrap-Around Fin*, Ph.D. thesis, Air Force Institute of Technology, WPAFB, OH, March 1997.

[11]Bendat, J. S. and Piersol, A. G., *Random Data: Analysis and Measurement Procedures*, J. Wiley, New York, 2nd ed., 1986.

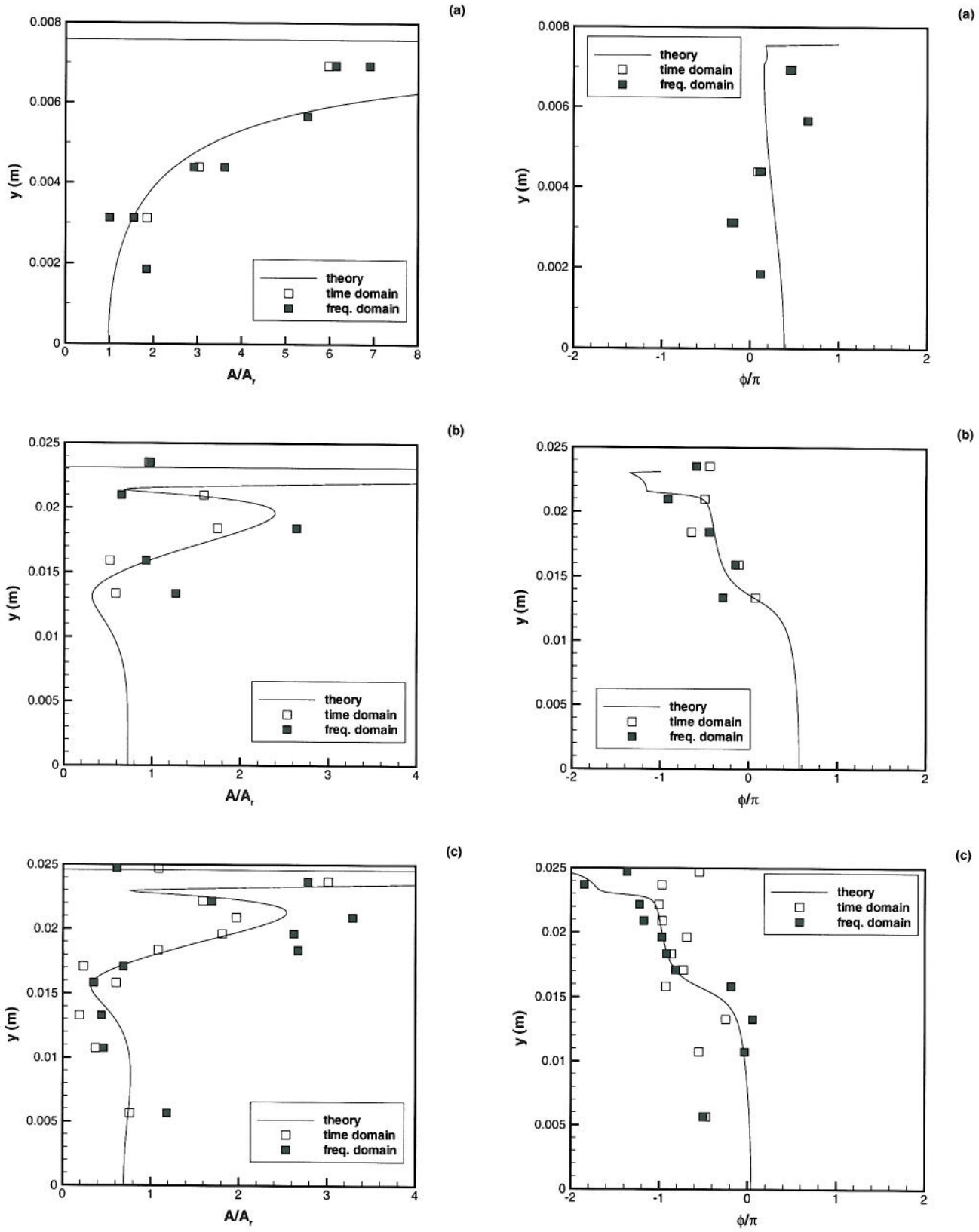

Fig. 12 Wall-normal survey of relative amplitude. (a) Station $x = 19.8$ mm (**0.78 in**). (b) Station $x = 60.5$ mm (**2.38 in**). (c) Station $x = 64.3$ mm (**2.53 in**).

Fig. 13 Wall-normal survey of relative phase. (a) Station $x = 19.8$ mm (**0.78 in**). (b) Station $x = 60.5$ mm (**2.38 in**). (c) Station $x = 64.3$ mm (**2.53 in**).